Solid State Science and Technology, Vol. 24, No 1 (2016) 14-29
ISSN 0128-7389 | *http://journal.masshp.net*

INVESTIGATION OF SCREEN-PRINTED METAL CONTACTS TO n-DOPED MULTI-CRYSTALLINE Si SUBSTRATE

Samir Mahmmod Ahmad[1,2], Wan Zulhafizhazuan[1], Cheow Siu Leong[1], Kamaruzzaman Sopian[1] and Saleem H. Zaidi[1]

[1] *Solar Energy Research Institute, Universiti Kebangsaan Malaysia, Bangi, Selangor, 43600, Malaysia*

[2]*Department of Physics, Faculty of Science, University of Mosul, 41002 Mosul, Iraq*

Corresponding author: samirasia60@yahoo.com

ABSTRACT

Ohmic metal contact formation to n and p-doped surfaces of a solar cell plays a central role in determining its series and shunt resistances. Rapid thermal annealing (RTA) based on conveyor-belt translation of the screen-printed wafers at elevated temperatures is the standard industrial practice for metal contact formation. In an industrial process, screen-printed wafer travels through multiple high temperature zones at controllable speeds to form low resistance ohmic contacts. In this study, inexpensive alternate RTA methods aimed at screen-printed electrical contact optimization as a function of the peak RTA temperature at fixed transit time have been investigated. Three different RTA systems were investigated: an industrial 6-zone conveyer belt furnace, a custom-designed 3-zone quartz 5”-diameter tube furnace, and a table-top 3”-diameter quartz tube system with computer-controlled bank of quartz lamps. Starting material was p-doped wafers with the bulk resistivity in ~ 1-3 ohm-cm range. Emitter formation was carried out using inexpensive, non-toxic spin-on phosphorous acid and conventional $POCl_3$ diffusion processes. The contact resistivity measurements were based on transmission line method (TLM). The lowest contact resistivities measured were: (a) ~ 2.0mΩ cm^2 for Ag and 412mΩ cm^2 for Al in industrial conveyor belt furnace at peak firing temperature of 860^{o}C, (b) ~ 4.1 mΩ.cm^2 for Ag and 77.7 mΩ.cm^2 for Al at the peak temperature of 925^o C in quartz tube furnace, and (c) ~ 1.2 m Ω.cm^2 for Ag and 63.5 mΩ.cm^2 for Al at the peak firing temperature of 780 ^{o}C in table-top RTA system. For Ag, the lowest contact resistance was achieved in the table-top RTA system, while for Al, the highest contact resistance was observed in the industrial conveyor belt six-zone furnace.

Keywords: solar cell; contact resistivity; screen printed metal pastes; transmission line method; rapid thermal annealing;

INTRODUCTION

Low resistance, ohmic metal-contact formation determines efficiency of the solar cell on account of sensitive dependence of fill factor on series and shunt resistances. Co-firing or annealing of the screen printed silver (Ag) to n-doped and Aluminium (Al) to p-doped crystalline Si surfaces is the prevalent industrial contact formation process. Following screen printing of the Ag and Al pastes on front and rear surfaces, the solar cell is first placed in a low temperature oven to drive-off solvents. This step is immediately followed by high temperature step in which both Ag and Al metal contacts to respective Si surfaces are created simultaneously [1,2]. This process is carried out in a conveyor belt furnace with IR quartz-halogen lamps as the heating source. This industrial-grade furnace is expensive and consumes excessive electricity. Alternate furnace designs with lower cost and energy usage are desirable to reduce process times as well as enhance efficiency.

In solar cells, low resistance ohmic contacts between silver paste/ n^+ emitter layer and Al paste/p^+-layer are needed to extract current from photo-generated electron-hole pairs. The methods to form ohmic contacts require (i) A metal with work function close to that of semiconductor [3], or (ii) Insertion of a thin layer of narrow band gap material between metal and semiconductor [4], or (iii) Increasing the semiconductor surface doping to enable tunnelling of electrons from conduction band [5]. In silicon solar cells, the typical emitter doping concentrations (N_D) are 1×10^{18} cm^{-3} < N_D < 1×10^{22}cm^{-3}, hence, the dominant current transport mechanisms are thermionic field emission (TFE) and field emission (FE)[6].

A highly effective method to evaluate the electrical properties of an ohmic contact is through its contact resistivity (ρ_c) [7]. Contact resistivity can be determined by the Transmission Line Method (TLM)[8]. TLM is based on the measurement of the electrical resistance between two ohmic contacts as function of the distance between them. By plotting resistivity as a function of distance between identical contact pads, contact resistivity can be determined.

The research work presented here is focused on TLM-based contact optimization as a function of peak Rapid thermal annealing (RTA) temperature during co-firing process for both front and rear surface screen-printed Ag and Al pastes on multi-crystalline silicon wafers. Boron-doped, mc-Si wafers were diffused using conventional gas-source $POCl_3$ to achieve an emitter with sheet resistance ~ 55Ω/sq and spin-on phosphoric acid emitter with sheet resistance ~ 70Ω/sq.

Description of TLM Masks:

Several designs of the TLM screen print masks, based on dimensions typical of industrially produced solar cells, were investigated. . The TLM 1 mask, described in Figure 1 (a), consisted of five patterns of six identical square contacts with same size (5×5 mm^2) but increasing distance between pads. The TLM 2 mask, described in Figure

1 (b), was composed of two patterns with eight identical contacts. The contacts dimensions of the first pattern (TLM21) was (2×10 mm^2) with separation d varying from 2.2 mm to 2.8 mm at 0.1 mm increment. The contact pad size of the third pattern (TLM22), also drawn in Figure1 (b), was (4×10 mm^2) with separation varying from 0.1 to 0.7 mm at an increment of 0.1 mm.

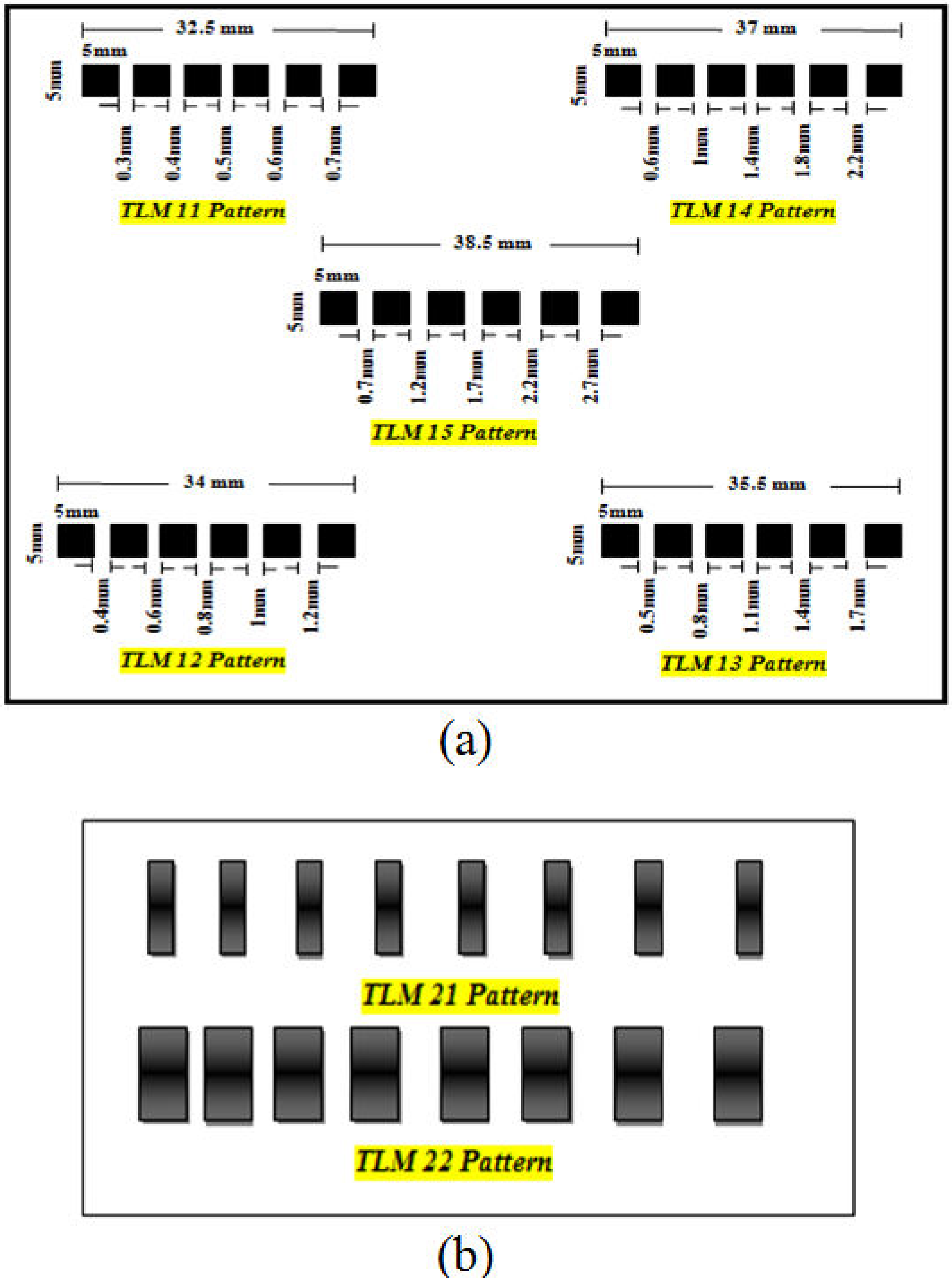

Figure 1: Schematic diagram of the TLM masks used, for resistivity measurements: (a) TLM 1 mask and (b) TLM 2 mask

EXPERIMENTAL

All screen-printing work was carried out on 10x10 cm^2, 200-µm thick, p-type multi-crystalline (mc) Si wafers with bulk resistivity in 1-3 Ω-cm range. The diffused wafers were divided to two groups. In the first group, a wet thermal oxidation process was used to grow thick (500 nm) SiO_2 films in conventional quartz tube furnace. Spin-on phosphoric acid diffusion was carried out on the front surface by first removing the oxide. Prior to spin-on process, hydrophilic surfaces were formed in $NH_4OH:H_2O_2:H_2O$ solution at (1:1:5) solution at 70 ^oC for 10 minutes. The Si wafers were subsequently spin-coated with the 20 % phosphoric acid solution at 2000 rpm for 20 sec followed by drying at 150 ^oC for 15 min in a thermal oven. The drive-in diffusion process was carried out at 875^oC for 30 min in a quartz tube furnace in N_2 ambient to form an emitter with sheet resistance of ~ 70 Ω/sq. Figure 2 illustrates the temperature profile used for the drive-in diffusion process. Following the diffusion process, front and back surface oxide films were removed in HF solution. For the second group, mc-Si wafers were doped with $POCl_3$ to form an emitter with sheet resistance of ~ 55 Ω/sq.

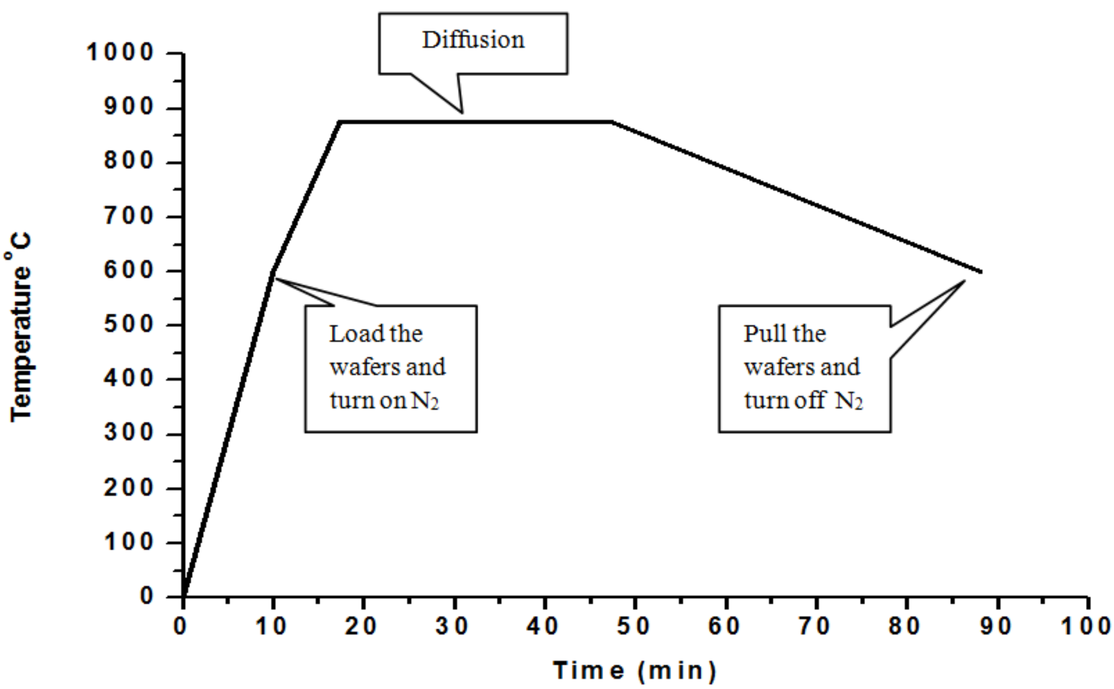

Figure 2: Schematic diagram of temperature profile used during for spin-on phosphorous drive-in diffusion at 875 ^oC

Screen printing process for TLM1 and TLM2 masks were carried out for front phosphorous-diffused side with Ag paste and non-diffused back side with Al paste. Screen-printed wafers were dried in a thermal oven for 10 minutes at 150 ^oC followed by high temperature annealing in three different geometrical configurations.

Solid State Science and Technology, Vol. 24, No 1 (2016) 14-29
ISSN 0128-7389 | *http://journal.masshp.net*

Six Zone Conveyor Belt IR Furnace:
Figure 3 illustrates 6-zone conveyor belt IR furnace manufactured by Radiant Technology Corporation (S-615C). The screen printed cells are placed on the conveyor belt as it moves from the heated region at a speed of 75 inches per minute. The peak firing temperatures at each of the six zones were varied in order to determine an optimum metal-contact annealing profile.

The set points for the 6-zone furnace have been summarized in table 1. Temperatures of five zones were kept fixed at 600^{o}C, 700^{o}C, 750^{o}C, 800^{o}C, 700^{o}C and only zone-4 temperature was varied from 800^{o}C to 900^{o}C at 20^{o}C increments; the belt speed was held constant at 75 ipm.

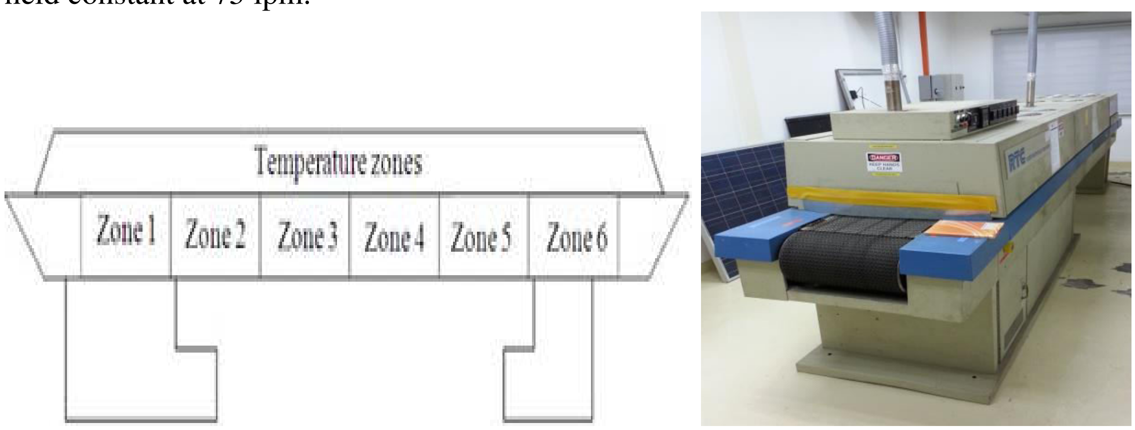

Figure 3: Schematic diagram of the industrial 6-zone conveyor belt RTC furnace (a) and picture of the 615 RTC system used for annealing (b)

Table 1: Conveyor Belt RTA Temperature Variation

No.	Zone 1	Zone 2	Zone 3	Zone 4	Zone 5	Zone 6
1				800^{o}C		
2				820^{o}C		
3	600^{o}C	700^{o}C	750^{o}C	840^{o}C	800^{o}C	700^{o}C
4				860^{o}C		
5				880^{o}C		
6				900^{o}C		

Custom-Designed Three Zone Quartz Tube Furnace:
This custom-designed RTA system was built with Lindberg/Blue M 1100^o C Digital Tube Furnace (STF55666C-1, 11KW) equipped with three independently controlled heating zones (Figure 4). This quartz tube furnace has been hooked up with controlled N_2 flow from one end with an exhaust system at the other end. Solar cells were placed on a Silicon Carbide paddle and moved across the 91-cm length of the heating zones with the help of a motor running at constant speed of 55 inches per minute.

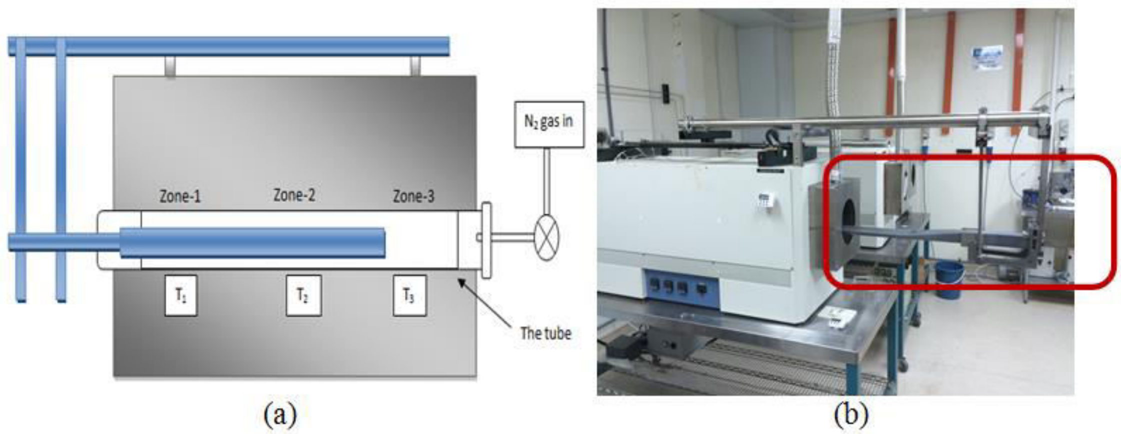

Figure 4: (a) Schematic diagram of the custom-designed 1100 °C 3-zone quartz tube furnace RTA and (b) picture of the actual system

The set points for Custom-designed 3- zone quartz tube furnace have been summarized in table 2. Temperatures at first and second temperature zones were kept fixed at 600°C while the third zone was varied from 875°C to 925°C at 25°C increments at a dwell time of 10 sec.

Table 2: Three Zone Furnace Temperature Variation

No.	Zone 1	Zone 2	Zone 3
1	600°C	600°C	850°C
2			875°C
3			900°C
4			925°C

Table Top RTA System

Figure 5 illustrates the schematic diagram of the custom-designed 3”-diameter table top RTA system. The system consists of a quartz chamber connected with gas inlet on its front and exhaust on the backside. The chamber is surrounded by insulated reflectors and heated by 2 tungsten halogen lamps placed at the top of the system and 4 tungsten halogen lamps placed at the bottom side of the tube. The thermal cycles are controlled by a programmed temperature controller. The temperature of the main process chamber of the system is measured with a K-type thermocouple placed at the centre of the tube.

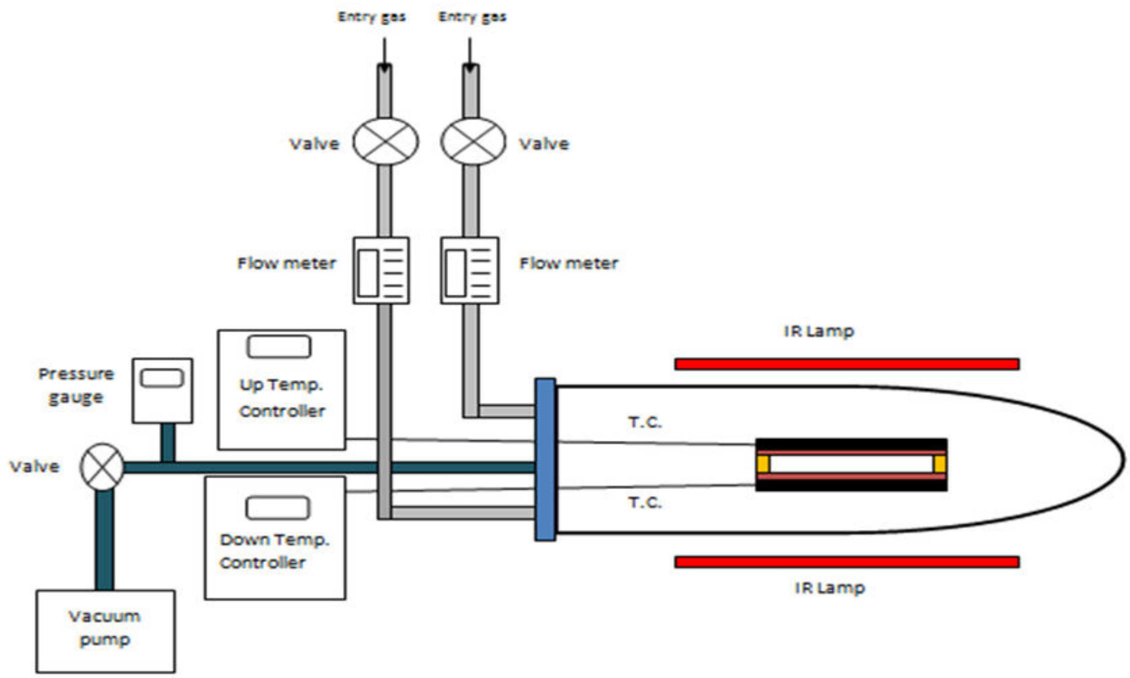

(a)

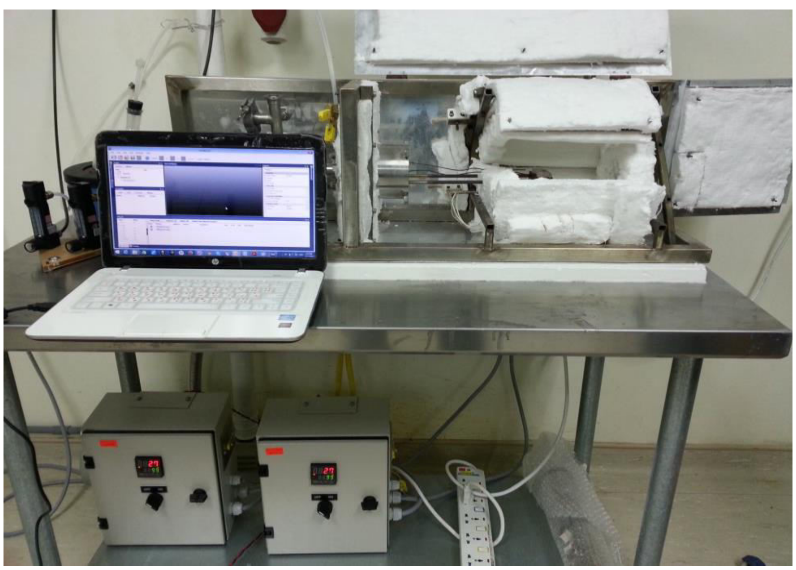

(b)

Figure 5: (a) Schematic diagram of the 3”-diameter table top RTA and (b) its picture

The set points for the table top RTA system were room temperature (RT) to 100^{o}C, 200^{o}C, 300^{o}C, 400^{o}C all at dwell time of 30 seconds, and finally the peak temperatures from 760^{o}C to 810^{o}C at increment of 10^{o}C with zero second dwell time as shown in table 3.

Table 3: Table Top RTA System Temperature Variation

No.	Set temperatures	
1		760°C (0sec)
2		770°C (0sec)
3	RT-100°C (30sec)-200°C (30sec)-300°C (30sec)-400°C	780°C (0sec)
4		790°C (0sec)
5		800°C (0sec)
6		810°C (0sec)

RESULTS AND DISCUSSION

In TLM method, the total resistance (R_t) between any two separate contacts is calculated by [9]

$$R_t = 2R_c + \frac{d.R_{sh}}{Z} \quad (1)$$

where R_c is the contact Resistance, R_{sh} is the sheet Resistance, and Z- is the width of the contact pad. The measured R_t is plotted as a function of distance (d) between contact pads as shown in Figure 6 (a). From the measured plot, three parameters can be extracted: R_c, from the intercept of the plot at d = 0 (Eq. 1), i.e., $R_t = 2R_c$. The transfer length (L_T) at $R_t = 0$ (Eq. 1) gives $d = 2L_T$ with the slope R_{sh}/Z while Z is independently measured (Fig 6(b)). The current flow from the diffused layer into the contact metal is regarded as a lateral. It is highest at the edges and drops towards the middle of the contact. Figure 7 indicates the current crowding effect at the periphery of the metal contact. The current flow from the doped thin layer into the contact metal is regarded as a lateral flow. It is highest at the edges and drops towards the middle of the contact. The distance at which the current density has dropped to 1/e from the initial value is called current transfer length (L_T) [10]. when this effect taken into account the contact resistance is [11]

$$R_c = (L_T/Z)R_{sh}\coth(L/L_T) \quad (2)$$

Where L is the length of the contact pads.
Two approximate solutions are of particular interest in Eq. 2:

1- If $L_T \leq 0.5\,L$, then the value of coth nears 1 and the ρ_c is [12]

$$\rho_c = R_c L_T Z \quad (3)$$

In this case, the ρ_c is independent of the contact length L.

2- If $L_T \geq 2L$, then coth nears the value of the factor in front of L and the ρ_c is[12]

$$\rho_c = R_c L\, Z \quad (4)$$

Solid State Science and Technology, Vol. 24, No 1 (2016) 14-29
ISSN 0128-7389 | *http://journal.masshp.net*

In this case, the ρ_c is dependent of the contact length L. For Silver paste, the value of L_T less than L, consequently predicated on the above conditions we used Eq. 3 to quantify ρ_c. For Al paste we used Eq. 4 due to dependence on entire contact length.

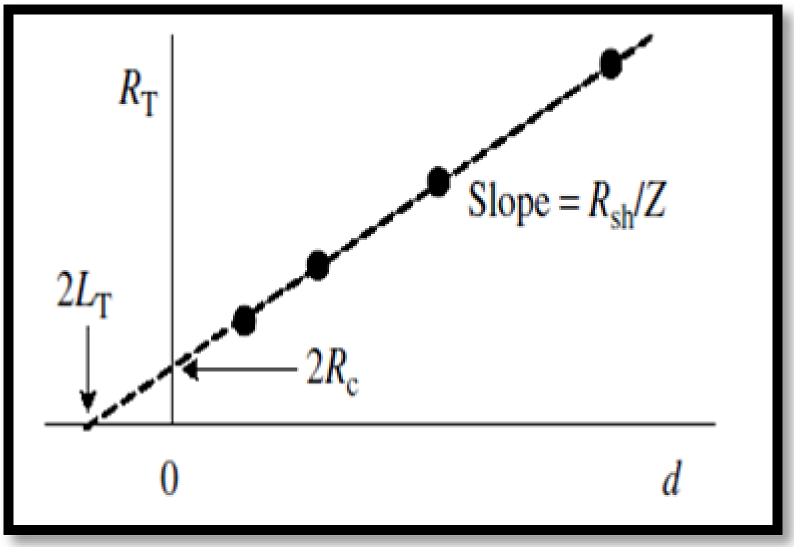

(a)

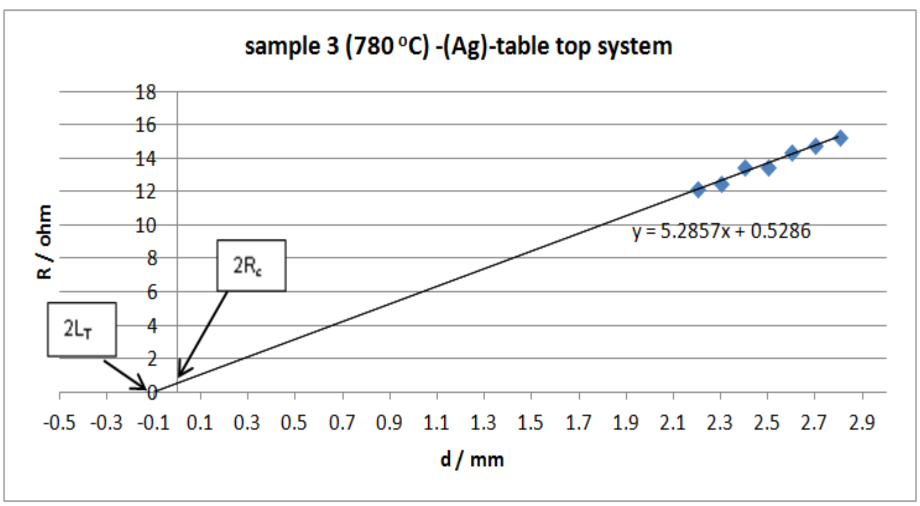

(b)

Figure 6: Plot of resistance R_t as a function of contact separation *d* (a) and experimentally measured resistance versus distance plot at peak firing temperature of 780^{o}C (b)

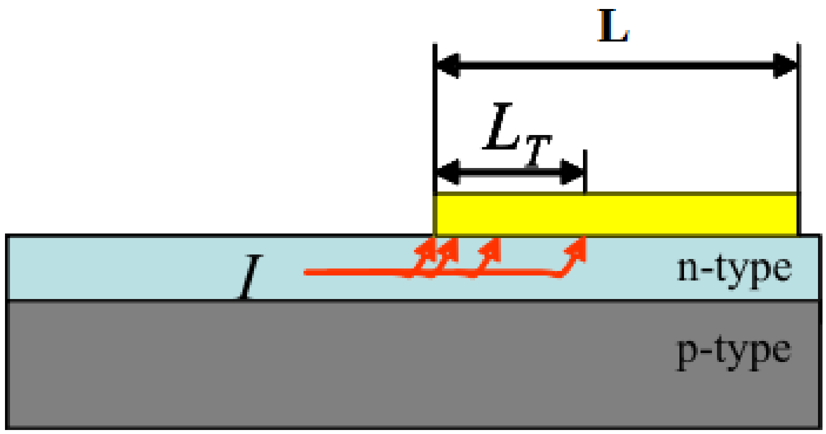

Figure 7: The current crowding effect as a result of the lateral current flow in the thin layer of the semiconductor region

Contact Resistivity in Conveyor Belt RTA

Annealing was optimized based on the temperature profiles identified in table 1. Table 4 summarizes averaged resistivity, while its plot is given by Figure 8. Figure 8 shows the measured data for ρ_c at different peak firing temperatures for both Ag and Al pastes. Contact resistivity, ρ_c, is reduced with increasing peak firing temperature until the it reaches the optimum value 860 ^oC, after which ρ_c increases. This means at 860 ^oC optimum screen printed metal contact has been achieved. The lowest ρ_c value measured was ~ 2 mΩ.cm^2 for front side-Ag paste and 412 mΩ.cm^2 for back side-Al paste at peak firing temperature 860 ^oC.

Table 4 Measured contact resistivity in conveyor RTA

	Contact Resistivity (mΩ.cm^2)					
	Peak Temp. 800^{o}C	Peak Temp. 820^{o}C	Peak Temp. 840^{o}C	Peak Temp. 860^{o}C	Peak Temp. 880^{o}C	Peak Temp. 900^{o}C
Ag paste	84.6	84.4	20.5	2.02	21.9	27.7
Al paste	766	715	696.5	412	506.2	715

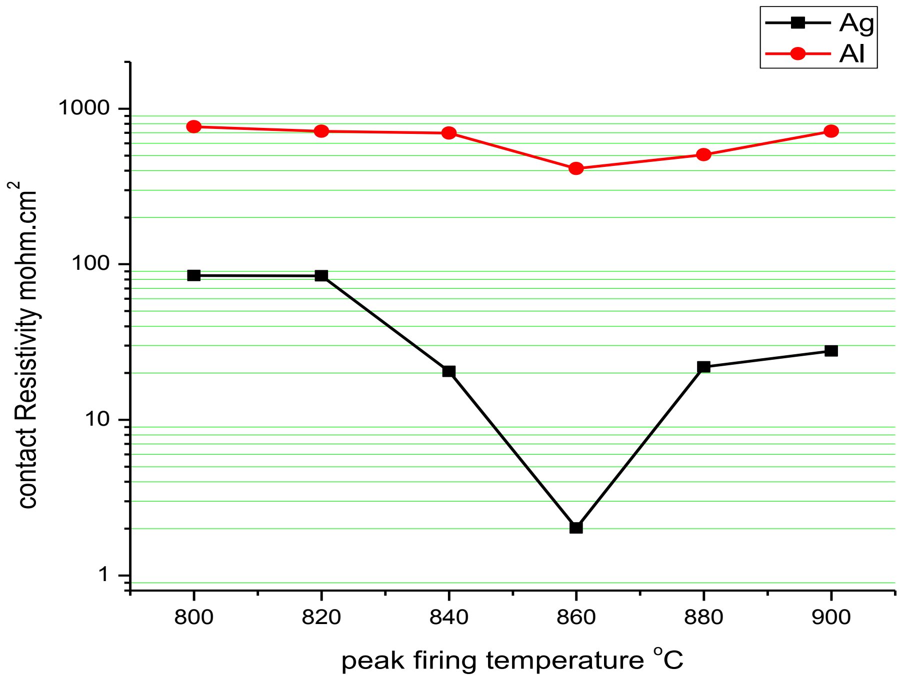

Figure 8: The contact resistivity variation with the peak firing temperature in RTA zone 4

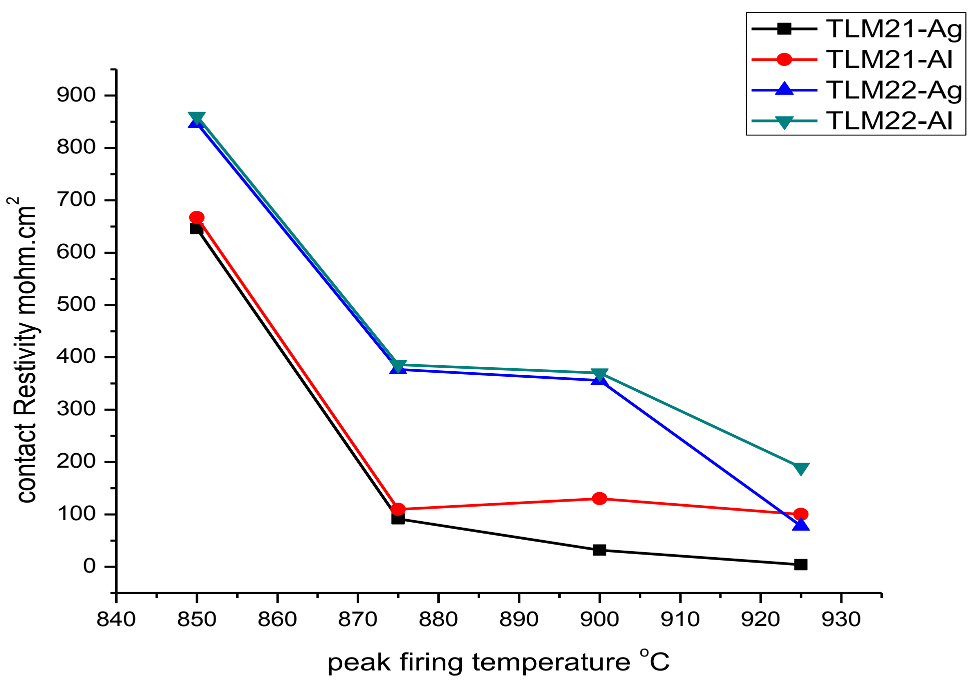

Figure 9: Contact resistivity variation as a function of peak firing temperature in custom-designed 3-Zone quartz tube furnace

Contact Resistivity in Custom-Designed 3-Zone Quartz Furnace

Two parameters influence the contact formation: (a) the peak temperature and (b) the dwell time at peak temperature. Following optimization with temperature parameters, it was determined that the best dwell time for this furnace was 10 seconds. Figure 9 plots the measured data for ρ_c as a function of peak firing temperature for both Ag and Al pastes for both TLM21 and TLM22 patterns. It is observed that ρ_c value for both TLM21pattern and TLM22 patterns decreases rapidly with increasing peak firing temperatures in ~ 850-880°C range; at higher temperatures up to 925°C, reduction is slow; therefore, optimum firing is between 880-925°C.

The plotted data in Figure 9 is summarized in Table 5. The lowest ρ_c values were achieved at peak firing temperature of 925 °C for both TLM21 pattern and TLM22 patterns for both Ag and Al contacts. For Ag, the lowest values were 4.1 mΩ.cm^2 and 77.7 mΩ.cm^2, and the respective values for Al were 100 mΩ.cm^2 and 190 mΩ.cm^2. Another interesting effect is related to scaling ratios. Table 6 summarizes resistivity ratios (TLM22/TLM21) for both Ag and Al contacts. It is noticed that for Ag contact, ratio increases as a function of temperature reaching a maximum of ~ 19 from the minimum value of 1.3. For Al contact, this effect is not pronounced, and the highest ratio value is ~ 3 at 900 °C.

Table 5: Measured Contact Resistivity in 3-Zone Quartz Tube Furnace

		Contact Resistivity (mΩ.cm^2)			
		Peak Temperature 850°C	Peak Temperature 875°C	Peak Temperature 900°C	Peak Temperature 925°C
TLM21	Ag paste	646	91.8	31.8	4.1
	Al paste	667	151	130	100
TLM22	Ag paste	847	377	356	77.7
	Al paste	860	386	370	190

Table 6: Variation of resistivity with TLM contacts for Ag and Al contacts for 3-Zone Furnace

Peak Temperature (°C)	Ratio TLM22/TLM21 for Ag	Ratio TLM22/TLM21 for Al
850	1.3	1.3
875	4.1	2.5
900	11.2	2.8
925	18.9	1.9

Contact Resistivity in Table-Top RTA System

Figure 10 plots the measured data for ρ_c as a function of peak firing temperatures for both Ag and Al pastes for both TLM21 and TLM22 patterns. It is observed that ρ_c, for both TLM21 and TLM22 patterns, is reduced with increasing peak firing temperature until reaches the lowest value at ~ 780 ^oC, after that it increases rapidly. This is may be due to metal penetrating the emitter layer causing leaky or shorted junctions.

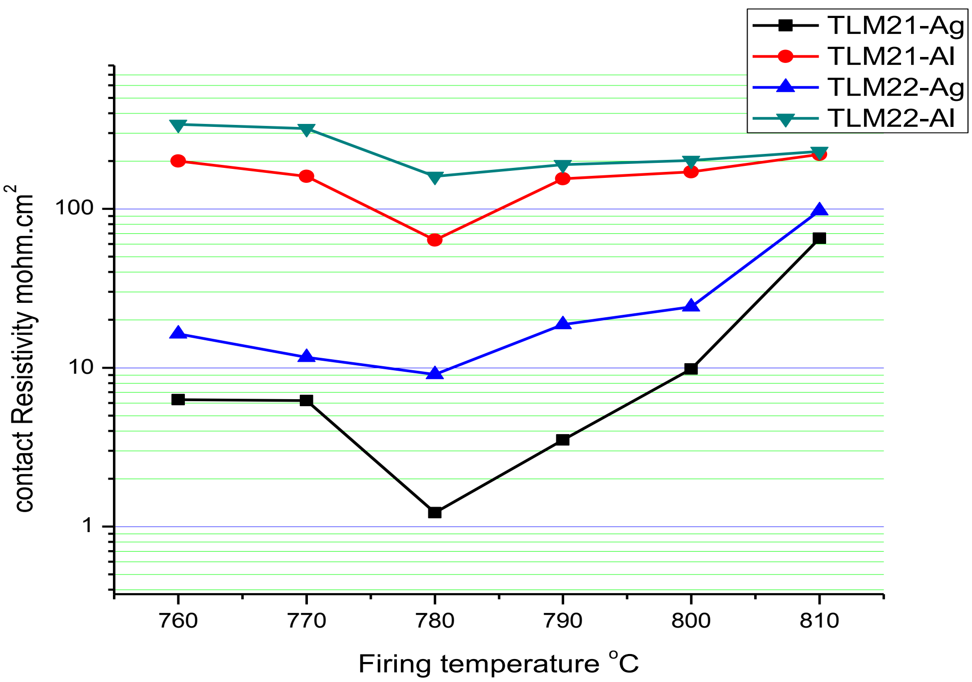

Figure 10: Contact resistivity variation with peak RTA temperature in the table-top system

Table 7 summarizes measured contact resistivity at peak firing temperatures varying from 760^{o}C to 810^{o}C. The minimum value of the contact resistivity was achieved at the peak temperature of 780^{o}C. For Ag contact, lowest resistivity values were 1.22mΩ.cm^2 and 63.5 mΩ.cm^2 and respective values for Al contact were 9.05mΩ.cm^2 and 160 mΩ.cm^2.

Table 8 summarizes resistivity ratios (TLM22/TLM21) for both Ag and Al contacts. It is noticed that for Ag contact, the ratio as a function of temperature reaches a maximum of ~ 7.4 at a peak firing temperature of 780 ^{o}C and then is reduced to ~ 1.5 at a peak firing temperature of 810 ^{o}C. For Al contact, this effect is not pronounced. The resistivity ratio increases as a function of temperature reaching a maximum of ~ 2.5 at a peak firing temperature of 780 ^{o}C and is then reduced slowly to ~ 1 at a peak temperature of 810 ^{o}C.

Table 7: Measured Contact Resistivity in Table-top RTA

		Contact Resistivity (mΩ.cm^2)					
		Peak Temp. 760^{o}C	Peak Temp. 770^{o}C	Peak Temp. 780^{o}C	Peak Temp. 790^{o}C	Peak Temp. 800^{o}C	Peak Temp. 810^{o}C
TLM21	Ag paste	6.3	6.2	1.22	3.5	9.8	65.4
	Al paste	200	160	63.5	155	171	220
TLM22	Ag paste	16.3	11.6	9.05	18.7	24.2	97.7
	Al paste	340	320	160	190	202	230

Table 8: Variation of resistivity with TLM contacts for Ag and Al contacts for Table-Top RTA

Peak Temperature (°C)	Ratio TLM22/TLM21 for Ag	Ratio TLM22/TLM21 for Al
760	2.6	1.7
770	1.9	2
780	7.4	2.5
790	5.3	1.2
800	2.4	1.2
810	1.5	1.0

Comparison of ratio data in tables 6 & 8 exhibits large variations as a function of temperature for Ag but not for Al. For Ag, this is explained in Eq. 3 in terms of the current transfer from semiconductor to metal that takes place over the transfer length L_T. Therefore, if ρ_c is sufficiently low, most of the current flow will take place near the edge of the metal contact, and L_T will be small. In contrast for high ρ_c, the L_T will be large. In a case of Al, dependence of the ρ_c on the contact area is dominant this is consistent with reported by Urrejola et al [13], who observed a dependence of the contact resistivity on the contact length but less on the firing temperature.

CONCLUSION

The focus of the research work presented here is on physical mechanisms and optimization of screen printed Ag and Al contact formation as function of peak RTA temperature in three different thermal configurations. Preliminary data illustrates that the lowest Ag contact resistivity is 1.2mΩ.cm^2 in table-top system at peak RTA temperature of 780^{o}C. This value is lower than measured 8.27mΩ.cm^2 at emitters of sheet resistance 60 Ω/sq[14]. For Al contact the lowest contact resistivity is 63mΩ.cm^2

in table-top system for contact length 2 mm at the same peak firing temperature. This value is lower than measured 17 $m\Omega.cm^2$ for laser-based contacts at 0.17 mm contact length [13] . An interesting effect relating to size effect was observed. The resistivity ratios for Ag increase with temperature with values as high as 19. In contrast, for Al, the ratios remain relatively invariant with a maximum of ~ 2.5. This variation may be attributed to the fact that contact resistivity is reduced with increasing peak firing temperature until it reaches the lowest as observed in Figs. 9 and 10. From Eq. 3, the current transfer length is reduced as well which leads to increase the scaling rate with increase firing temperature. The research work indicates that the lowest contact resistivities are achieved at the lowest temperature table-top RTA system. Contact resistances for both conveyor RTA and custom-designed RTA are also comparable, therefore, both (table-top and custom-designed) RTA systems offer highly attractive low-cost alternatives to expensive and high thermal budget industrial conveyor RTA furnaces. A contact resistivity less than $2m\Omega\text{-}cm^2$ is sufficient to for high efficiency, screen-printed solar cells in one sun applications of the screen-printed Si solar cells [10,11];thus, alternate RTA system are offer attractive low cost options for solar cell manufacturing.

REFERENCES

[1]. I. B. Cooper, K. Tate, J. S. Renshaw, A. F. Carroll, K. R. Mikeska, R. C. Reedy, A. Rohatgi, *IEEE J. Photovoltaics.* **4** 134–141 (2014)

[2]. D. M. Huljic, D. Biro, R. Preu, C. C. Castillo, R. Ludemann, Rapid thermal firing of screen printed contacts for large areacrystalline silicon solar cells, Conf. Rec. Twenty-Eighth IEEE Photovolt. Spec. Conf. Cat. No.00CH37036 (2000) 379–382.

[3]. J. Lee, Y.-J. Lee, M. Ju, K. Ryu, B. Kim, J. Yi, *Nanoscale Res. Lett.* **7** 32 (2012)

[4]. S. M. Sze, K. K. Ng, Physics of Semicondcutor Devices, third ed., John Wiley & Sons, Inc., Hoboken, New Jersey, 2007.

[5]. A. Ebong, S. Member, *J. Appl. Phys.* 102–109 (2012)

[6]. M. Hörteis, T. Gutberlet, A. Reller, S. W. Glunz, *Adv. Funct. Mater.* **20** 476–484 (2010)

[7]. M. Melczarsky, G. Gallego Garcia, N. E. Posthuma, E. Van Kerschaver, G. Beaucarne, Contact resistance measurement techniques for Ag thick-film screen-printed contacts to solar cells, Conf. Rec. IEEE Photovolt. Spec. Conf. (2009) 000960–000963.

[8]. P. N. Vinod, *J. Mater. Sci. Mater. Electron.* **18** 805–810 (2007)

[9]. D. K. Schroder, Semiconductor Material and Device Characterization, third ed., John Wiley & Sons, Inc., Hoboken, New Jersey, 2006.

[10]. P. N. Vinod, *J. Mater. Sci. Mater. Electron.* **22** 1248–1257 (2011)

[11]. D. K. Schroder, D. L. Meier, *IEEE Trans. Electron Devices. ED* **31** 637–647 (1984)

[12]. A. Goetzberger, J. Knobloch, B. Voss, Crystalline Silicon Solar Cells, John Wiley & Sons Ltd., England, 1998.

[13]. E. Urrejola, K. Peter, H. Plagwitz, G. Schubert, J. Appl. Phys. **107** 1–5 (2010)

[14]. S. Kim, S. Park, Y. Do Kim, S. Bae, H. Boo, H. Kim, K. D. Lee, S. J. Tark, D. Kim, *J. Nanosci. Nanotechnol.* **14** 7774–7778 (2014)